

MEGAMASER DISKS REVEAL A BROAD DISTRIBUTION OF BLACK HOLE MASS IN SPIRAL GALAXIES

J. E. GREENE¹, A. SETH², M. KIM³, R. LÄSKER, A. GOULDING¹, F. GAO⁶, J. A. BRAATZ⁴, C. HENKEL⁵, J. CONDON⁴, K. Y. LO⁴, W. ZHAO

Draft version September 1, 2018

ABSTRACT

We use new precision measurements of black hole masses from water megamaser disks to investigate scaling relations between macroscopic galaxy properties and supermassive black hole (BH) mass. The megamaser-derived BH masses span $10^6 - 10^8 M_{\odot}$, while all the galaxy properties that we examine (including total stellar mass, central mass density, and central velocity dispersion) lie within a narrower range. Thus, no galaxy property correlates tightly with M_{BH} in $\sim L^*$ spiral galaxies as traced by megamaser disks. Of them all, stellar velocity dispersion provides the tightest relation, but at fixed σ_* the mean megamaser M_{BH} are offset by -0.6 ± 0.1 dex relative to early-type galaxies. Spiral galaxies with non-maser dynamical BH masses do not appear to show this offset. At low mass, we do not yet know the full distribution of BH mass at fixed galaxy property; the non-maser dynamical measurements may miss the low-mass end of the BH distribution due to inability to resolve their spheres of influence and/or megamasers may preferentially occur in lower-mass BHs.

1. INTRODUCTION

For more than a decade, we have studied the relationship between the stellar velocity dispersion σ_* of a galaxy bulge and the central supermassive black hole (BH) mass M_{BH} (e.g., Tremaine et al. 2002). As more dynamical M_{BH} are measured, particularly at the highest M_{BH} (e.g., McConnell & Ma 2013) and in spiral galaxies (Greene et al. 2010), it has become clear that the relationship between M_{BH} and σ_* has more scatter and more structure than was originally thought (Kormendy & Ho 2013).

BH mass does not correlate strongly with total galaxy mass (e.g., Reines & Volonteri 2015), nor does it appear to correlate with circular velocity (and thus by inference dark matter halo mass; Sun et al. 2013). It is possible that M_{BH} is built up along with the bulge mass. However, in late-type galaxies where there is clear evidence for ongoing bulge growth, M_{BH} appear to be systematically lower than expected based on BH-bulge relations in early-type galaxies (e.g., Läscher et al. 2016). Here, we use megamaser disks that reside well within the BH sphere of influence to probe the distribution of M_{BH} in spiral galaxies.

We assume an H_0 of $70 \text{ km s}^{-1} \text{ Mpc}^{-1}$ (Dunkley et al. 2009), consistent with all of the H_0 measurements from megamaser disk galaxies measured to date (e.g., Kuo et al. 2015).

2. MEGAMASER DISK GALAXIES, SAMPLE, AND OBSERVATIONS

Stellar and non-maser gas dynamical methods yield the majority of dynamical M_{BH} , but they are limiting both in spatial resolution and in ability to cleanly measure M_{BH} in all galaxy types. Due to the need to resolve the gravitational sphere of influence, these methods currently cannot reach $M_{\text{BH}} < 10^7 M_{\odot}$ at the distance of Virgo. Dust, ongoing star formation, and non-

axisymmetric potentials such as bars also complicate efforts to get M_{BH} in late-type galaxies. Megamaser disks circumvent these problems and provide the most accurate and precise extragalactic M_{BH} measurements.

Circumnuclear H_2O megamasers often trace Keplerian rotation around the supermassive BH at radii of $\sim 0.2 - 1 \text{ pc}$ (e.g., Miyoshi et al. 1995). Sensitive surveys, enabled primarily by the Green Bank Telescope (GBT), and micro-arcsecond accurate mapping of the disks with the Very Long Baseline Array (VLBA), the Jansky Very Large Array (JVLA), the GBT, and/or the 100-m Effelsberg telescope have yielded more than 150 megamaser galaxies, of which at least 34 harbor megamaser disks (e.g., Pesce et al. 2015). The host galaxies are $\sim L^*$ spirals with Hubble types S0-Sbc, while the derived M_{BH} have values ranging from $10^6 - 10^8 M_{\odot}$ (e.g., Greene et al. 2010; Kuo et al. 2011). Here we add σ_* measurements for seven galaxies, whose M_{BH} are presented in Gao et al. (2016), Gao et al. in preparation, and Zhao et al. in preparation (Table 1).

2.1. Comparison Galaxy Sample

We consider only galaxies with dynamical M_{BH} measurements. We start with the recent compilation from Saglia et al. (2016, 97 galaxies) plus a new megamaser disk mass for IC2560 (Wagner et al. in preparation). Of these 98, 13 are megamaser disks. We add non-maser dynamical masses for NGC 4395 (den Brok et al. 2015), and the interesting outliers NGC 1271 (Walsh et al. 2015), NGC 1277 (Walsh et al. 2016), and NGC 1600 (Thomas et al. 2016) for a total of 102 literature sources and a final sample of 109 galaxies including our 7 new megamaser disks (Table 1). There are a total of 20 megamaser disk galaxies and 17 late-type (non-S0) non-maser spiral galaxies. When we discuss stellar masses (M_*), we refer to the 67

¹Department of Astrophysics, Princeton University

²University of Utah, Salt Lake City, UT 84112, USA

³Korea Astronomy and Space Science Institute, Daejeon 305-348, Korea; University of Science and Technology, Daejeon 305-350, Korea

⁴National Radio Astronomy Observatory, 520 Edgemont Road, Charlottesville, VA 22903, USA

⁵Max-Planck-Institut für Radioastronomie, Auf dem Hügel 69, D-53121 Bonn, Germany; Astronomy Department, King Abdulaziz University, P.O. Box 80203, Jeddah 21589, Saudi Arabia

⁶Key Laboratory for Research in Galaxies and Cosmology, Shanghai Astronomical Observatory, Chinese Academy of Science, Shanghai 200030, China; National Radio Astronomy Observatory, 520 Edgemont Road, Charlottesville, VA 22903, USA; Graduate School of the Chinese Academy of Sciences, Beijing 100039, China

galaxies that have imaging from the Sloan Digital Sky Survey (SDSS; York et al. 2000).

2.2. Spectroscopic Observations

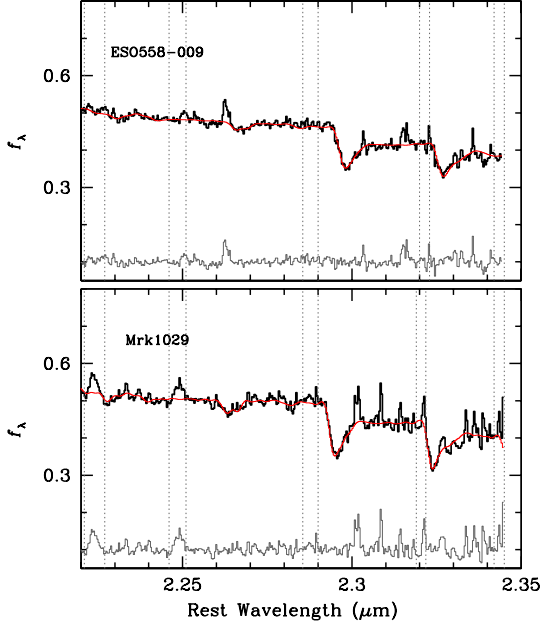


FIG. 1.— Fits to the observations of ESO 558–009 and Mrk 1029 from Triplespec (§2.2). The data are shown in black (in f_λ units of $\text{erg s}^{-1} \text{cm}^{-2} \text{\AA}^{-1}$ arbitrarily scaled), the best-fit pPXF model in red, and residuals in thin black at the bottom. Masked regions corresponding to emission lines are indicated with vertical dashed lines. Unmasked spikes are the result of imperfect sky subtraction.

The σ_* presented here are measured from three data sets. Two galaxies (NGC 1320, NGC 5495) were observed with the B&C spectrograph on the Dupont telescope at Las Campanas Observatory using a $2''$ slit (Greene et al. 2010). These spectra have an instrumental resolution of $\sigma_r \approx 120 \text{ km s}^{-1}$ and a wavelength range of $3400\text{--}6000\text{\AA}$. NGC 1320 is only marginally spectroscopically resolved, while NGC 5495 is well-resolved, but we are able to recover reliable dispersions at or slightly below the instrumental resolution (Greene et al. 2010). We extracted spectra within a $2''$ aperture to perform our measurements. The reductions are described in detail in Greene et al. (2010). Standard flat-field, bias, wavelength calibration, flux, and telluric correction were performed within IRAF. Each galaxy was observed for 1.3 hr, yielding signal-to-noise ratios of $\sim 100 \text{ pixel}^{-1}$ (see example fits to similar objects in Greene et al. 2010).

Two galaxies (Mrk1029, ESO558–G009) have σ_* measurements from the cross-dispersed near-infrared spectrograph Triplespec (Wilson et al. 2004) on the 3.5m telescope at Apache Point. Triplespec has a wavelength range of $0.9\text{--}2.4\mu\text{m}$ with a spectral resolution of $\sigma_r \approx 37 \text{ km s}^{-1}$, far higher than the internal σ_* of the galaxies. We observed with the $1''1$ slit oriented along the major axis of each galaxy; again we extracted data within a $2''$ aperture. We nodded off the galaxy by $1\text{--}3'$ to measure the sky, and at least once an hour we observed an A0V star ($10 < H < 6 \text{ mag}$) at similar airmass to serve as a spectrophotometric standard and to facilitate telluric correction. Integration times ranged from 0.5–1.5 hr, yielding signal-to-noise ratios of $\sim 50 \text{ pixel}^{-1}$ (Fig. 1).

Table 1. Galaxy Sample

Galaxy (1)	D (2)	Type (3)	M_{BH} (4)	σ_* (5)	M_{tot} (6)	$M_{1\text{kpc}}$ (7)	Meth (8)
Mrk1029	124.0	3p	6.28 ± 0.13	2.12 ± 0.05	10.57 ± 0.05	10.08 ± 0.06	maser
NGC1320	49.1	3p	6.74 ± 0.16	2.15 ± 0.05	maser
J0437+2456	66.0	3p	6.45 ± 0.03	2.04 ± 0.05	10.57 ± 0.22	10.04 ± 0.04	maser
ESO558–G009	102.5	3p	7.22 ± 0.03	2.23 ± 0.05	maser
UGC6093	150.0	3p	7.41 ± 0.02	2.19 ± 0.05	11.21 ± 0.05	10.19 ± 0.08	maser
NGC5495	93.1	3p	7.00 ± 0.05	2.22 ± 0.05	maser
NGC5765b	113.0	3p	7.64 ± 0.05	2.21 ± 0.05	maser
IC2560	41.8	3	6.64 ± 0.06	2.15 ± 0.03	maser
NGC1068	15.9	3p	6.92 ± 0.25	2.18 ± 0.02	10.42 ± 0.58	10.63 ± 0.06	maser
NGC1194	58.0	2	7.85 ± 0.05	2.17 ± 0.07	10.81 ± 0.08	10.19 ± 0.09	maser
NGC2273	29.5	3p	6.93 ± 0.04	2.10 ± 0.03	maser
UGC3789	49.9	3p	6.99 ± 0.09	2.03 ± 0.05	maser
NGC2960	67.1	2p	7.03 ± 0.05	2.22 ± 0.04	10.98 ± 0.03	10.40 ± 0.03	maser
NGC3079	15.9	3p	6.40 ± 0.05	2.16 ± 0.02	10.38 ± 0.05	9.85 ± 0.09	maser
NGC3393	49.2	3p	7.20 ± 0.33	2.17 ± 0.03	maser
NGC4258	7.3	3	7.58 ± 0.03	2.06 ± 0.04	10.52 ± 0.04	10.00 ± 0.05	maser
Circinus	2.8	3p	6.06 ± 0.10	1.90 ± 0.02	maser
NGC4388	16.5	3p	6.86 ± 0.04	2.00 ± 0.04	10.43 ± 0.05	9.73 ± 0.06	maser
NGC6264	147.6	3p	7.49 ± 0.05	2.20 ± 0.04	11.01 ± 0.09	9.92 ± 0.08	maser
NGC6323	113.4	3p	7.00 ± 0.05	2.20 ± 0.07	11.03 ± 0.09	9.97 ± 0.05	maser
MW	0.008	3p	6.63 ± 0.05	2.02 ± 0.08	star
NGC0221	0.8	1	6.39 ± 0.19	1.89 ± 0.02	star
NGC0224	0.8	3	8.15 ± 0.16	2.23 ± 0.02	star
NGC0307	52.8	2	8.60 ± 0.06	2.31 ± 0.01	10.81 ± 0.04	10.38 ± 0.03	star

Note. — Col. (1): Galaxy. We show the maser galaxies presented in this work (first seven), followed by literature maser galaxies, and then the remaining literature (§2.1). Logarithmic errors have been symmetrized. This shortened table is just a guide to form and content. Col. (2): Distance (Mpc). Col. (3): Morphological group (1 = elliptical, 2 = S0, 3 = spiral). Galaxies assumed to harbor pseudobulges (based on Saglia et al. 2016 and assuming that all of our new megamasers harbor a pseudobulge component) are marked with a ‘p’. Col. (4): Log black hole mass (M_\odot). Col. (5): Log stellar velocity dispersion (km s^{-1}), derived from this paper for the first seven objects, newly presented here. The rest of the measurements are taken from Saglia et al. (2016), aside from NGC 4395, NGC 1271, NGC 1277, and NGC 1600; see §2.1. Col. (6): Log total stellar mass (M_\odot). Col. (7): Log stellar mass (M_\odot) contained within 1 kpc. Col. (8): Method used to measure the black hole mass.

We performed standard data reduction procedures using custom software written for Triplespec based on the Spextool package (Vacca et al. 2003; Cushing et al. 2004), which performed flat-fielding, wavelength calibration, bias, dark, and atmospheric air-glow subtraction. Nonlinearity corrections were applied, and the spectra are traced and optimally extracted (Horne 1986). The spectra were combined using a robust error clipping at each pixel. Flux calibration utilized observations of A0 telluric standards (Vacca et al. 2003).

Finally, three galaxies (J0437+2456, NGC 5765b, UGC 6093) have spectra from the SDSS. They have a spectral resolution of $\sigma_r \approx 65 \text{ km s}^{-1}$ (resolving our galaxies well) and cover a range of $3800\text{--}9200\text{\AA}$. The fiber has a $3''$ diameter, roughly matched to the extraction apertures used above.

3. ANALYSIS

3.1. Stellar Velocity Dispersions

We measure σ_* using direct pixel fitting implemented by the publicly available pPXF code (Cappellari & Emsellem 2004). We measure only the first two moments of the line-of-sight velocity distribution (V and σ_*). To account for differences in flux calibration and reddening, we also include a fourth-order multiplicative polynomial.

For the two optical spectrographs, we use spectral templates from Valdes et al. (2004), which have a higher spectral resolution than the galaxy observations ($\sigma_r \approx 24 \text{ km s}^{-1}$). The code solves for the optimal set of template weights over the spectral range of $4000\text{--}5400\text{\AA}$. We experiment with three other narrower spectral windows, and find agreement within $\sim 20\%$ for σ_* between the different regions.

Our near-infrared spectral template stars are taken from Wallace & Hinkle (1996) and have a spectral resolution of $\sim 33 \text{ km s}^{-1}$ in the K -band. The NIR spectra cover $YJHK$. We derive the most stable σ_* measurements from the CO bandheads

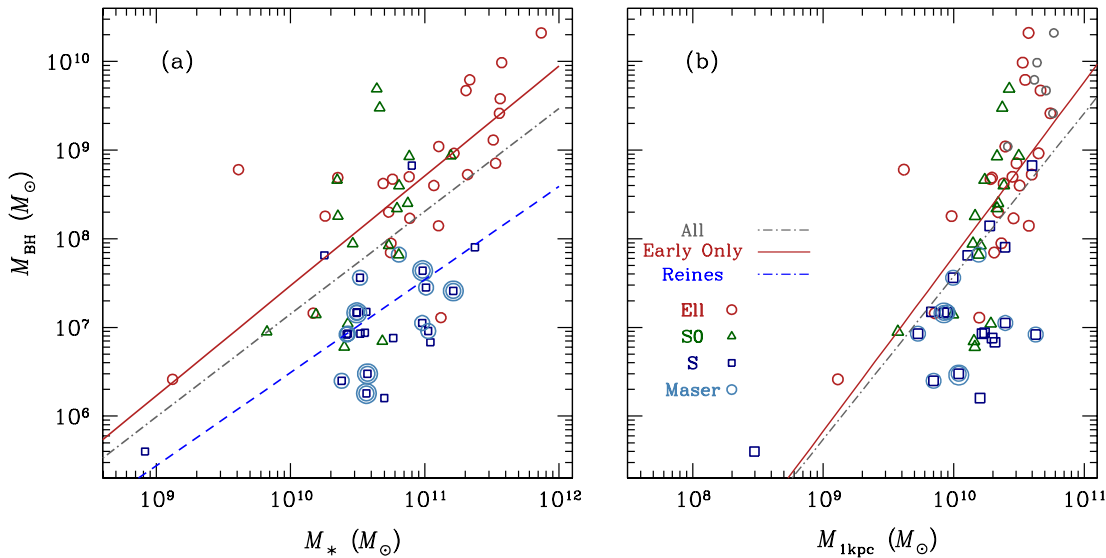


FIG. 2.— (a): Relationship between M_{BH} and M_* . We show elliptical (red circles), S0 (green triangles), spiral (blue squares), and megamaser disk (blue circles) galaxies. Double circles indicate our new measurements. We show fits to the full sample (grey dot-dashed), the early-types (red solid) and the Reines & Volonteri (2015) fit (blue dashed). (b): The relationship between M_{BH} and mass enclosed within 1 kpc. Symbols as at left. In grey we show the galaxy mass “corrected” for core-scouring (e.g., Rusli et al. 2013). Galaxies with radii $< 2''$ are excluded.

in the K -band (2.2–2.35 μm). The H -band data proved hard to fit due to spectral differences between the galaxies and our template stars.

3.2. Uncertainties in σ_*

The errors on σ_* are measured via bootstrapping; the best-fit models are combined with Gaussian-random noise of the proper amplitude to simulate the data and these are refit to generate a distribution in V and σ_* (Table 1). We also compare our observations with the σ_* measurements published by the Hobby Eberly Telescope Massive Galaxy Survey (HETGMS; van den Bosch et al. 2015). Taking the eight megamaser galaxies in common between HETGMS and the σ_* published in Greene et al. (2010) or presented here, we find $(\langle \sigma_{\text{HETGMS}} - \sigma_{\text{Thiswork}} \rangle / \sigma_{\text{HETGMS}}) = -0.03 \pm 0.13$. We set 13% as a floor on the measured uncertainty.

Aperture corrections are a significant source of systematic uncertainty. In ellipticals, σ_* is typically measured within a fixed fraction of R_e , which is challenging to measure in spiral bulges. Furthermore, σ_* profiles are more complex and V/σ is typically higher in spiral bulges, even when the large-scale disk is excluded, as here (e.g., Falc3n-Barroso et al. 2006; Greene et al. 2014). We do not correct σ_* for rotation, but we estimate the magnitude of such a correction as follows. Typical spirals have $V/\sigma_* \approx 0.3$ within 1–2'' (Falc3n-Barroso et al. 2006). Removing the rotation in quadrature moves the spirals toward the $M_{\text{BH}} - \sigma_*$ relation of ellipticals (e.g., Bennert et al. 2015). On the other hand, elliptical galaxies also typically rotate (e.g., Emssellem et al. 2007) so there is no strong scientific justification to remove this component of dynamical support only in the spiral galaxies.

3.3. Stellar Masses

In addition to σ_* , we calculate stellar masses (M_*) for the 67 galaxies that lie within the SDSS footprint using linear relationships between color and M/L from Bell et al. (2003). To estimate an allowed range of M_* , for each galaxy we calculate 12 possible stellar masses using the four SDSS Petrosian

colors to derive M/L , combined with the robustly measured g , r , and i -band luminosities. We average these estimates and take the standard deviation to estimate an error – this error is larger in systems with a wide mix of stellar populations and/or dust, where blue and red colors provide quite different M/L estimates.

We calculate M_* for the entire galaxy and within $r < 1$ kpc ($M_{1\text{kpc}}$). The mass within a fixed physical aperture is a crude but non-parametric estimate of the central stellar density, and might correlate better with M_{BH} than the total M_* . It is also a simple measurement relative to M_{bulge} , σ_* , or even M_* . We measure $M_{1\text{kpc}}$ from the SDSS data using the luminosity within a central circular aperture. We exclude galaxies where the aperture is $< 2''$, which are limited by the SDSS seeing.

3.4. Mass Uncertainties

Photometric stellar masses contain many uncertainties, including aperture effects, projection effects, and the contribution of nebular emission from an active nucleus (for the megamaser disk galaxies). The latter effect we mitigate by taking an average over multiple filters. We find only small differences when we test elliptical apertures for a subset of the galaxies (~ 0.2 mag), and removing edge-on galaxies does not change the result. We also explore whether our results are biased by using projected quantities. For the high-mass, high-S3rsic index galaxies, we analytically deproject the central mass (Bezanson et al. 2009) using the single-S3rsic fits from the NSA catalog. We reproduce our aperture measurements within 0.1 dex, with no systematic dependence on mass or n . Deprojection uncertainties may play a larger role for the pseudobulges, particularly for nearly edge-on inclinations. We explore the importance of the inclination using ellipse fitting to our HST data for the maser galaxies (Greene et al. 2014; L3sker et al. 2016) and find that the differences between circular and elliptical apertures are never larger than 0.2 mag, translating into < 0.1 dex in stellar mass.

Hardest to quantify are the errors incurred from our mass estimation techniques, but overall it has been shown that single-

color conversions (§3.3) return an unbiased stellar mass (Roediger & Courteau 2015).

4. EXPLORING BLACK HOLE-GALAXY CORRELATIONS

In Figure 2a, we show the relationship between M_{BH} and M_* . We fit all relations in this paper using the Bayesian line-fitting code of Kelly (2007), taking into account uncertainties in both M_{BH} and the galaxy properties. We fit a log-linear model with $\log(M_{\text{BH}}/M_\odot) = \alpha + \beta \log(X/X_0) + \epsilon$, with X being M_* , $M_{1\text{kpc}}$, or σ_* and X_0 near the center of the distribution (Table 2).

We find ~ 1 dex scatter in the relation between M_* and M_{BH} . At a stellar mass of $\sim 10^{11} M_\odot$, M_{BH} spans a range from 10^6 to $10^9 M_\odot$, and spiral galaxies tend to have lower M_{BH} than elliptical galaxies at similar M_* . We have long known that BHs correlate better with galaxy bulges than with M_* , disk mass (e.g., Gebhardt et al. 2003), or asymptotic circular velocity (e.g., Sun et al. 2013).

Original interpretations of the BH-bulge scaling relations posited that energy released during active phases of BH growth acted on galaxy-wide gas reservoirs, thus impacting the future growth of the galaxy (e.g., Springel et al. 2005). The BHs in the megamaser disk galaxies are too large to be primordial seeds (e.g., Volonteri 2010), so they have certainly undergone some accretion episodes, but the lack of correlation with M_* strongly suggests that BH growth does not remove gas from galactic disks (i.e., does not act beyond bulge scales). After removing the disk component, we still see considerable scatter between M_{BH} and bulge properties in late-type spiral galaxies, even when we attempt to isolate the “classical” bulge component from the nuclear disks, rings, and bars that characterize “pseudobulges” (Läscher et al. 2016; Saglia et al. 2016).

4.1. A Local Relationship with Central Density

Recent work has found that central mass density (stellar mass within 1 kpc, $M_{1\text{kpc}}$) is a strong indicator of the star formation history of a galaxy (e.g., Barro et al. 2015), with high central stellar density and galaxy quenching going hand in hand. Exactly what terminates star formation in dense galaxies remains unknown, but one possibility is feedback from supermassive BHs, which may grow along with dense cores. Thus, we consider a local relationship between M_{BH} and the mass enclosed within 1 kpc (Figure 2b).

A local relationship between M_{BH} and stellar mass is cheap to measure (§3.3) and relatively easy to compare with simulations (see Reines & Volonteri 2015). Such a local relationship might arise if the gas supply to the galaxy center determines both the central star formation rate and the overall rate of BH growth, and BH growth is self-regulated (e.g., Debuhr et al. 2010), or if the accretion disk is fed locally by stars rather than gas accretion (Miralda-Escudé & Kollmeier 2005).

The $M_{\text{BH}}-M_{1\text{kpc}}$ relation is shown in Figure 2b. We do observe an overall correlation between $M_{1\text{kpc}}$ and M_{BH} . However, the scatter is substantial (0.8 dex; Table 2), and the dynamic range in $M_{1\text{kpc}}$ is limited, causing a very steep scaling between $M_{1\text{kpc}}$ and M_{BH} . At the highest masses, core scouring (e.g., Rusli et al. 2013) tends to artificially decrease the central mass density. We “correct” the most massive galaxies for core scouring in Fig. 2b by adding the M_{BH} to the central mass, but our fits do not change.

⁷Taking the identifications from Saglia et al. 2016 for the literature sources and taking all of our new galaxies to harbor some secularly evolving component based on our new *HST* imaging; Pjanka et al. in preparation.

Table 2. Fit Parameters

Sample (1)	N (2)	α (3)	β (4)	ϵ (5)
$M_{\text{BH}}-M_{\text{tot}}$				
ALL	67	7.20 ± 0.26	1.2 ± 0.2	0.9 ± 0.3
EARLY	43	7.50 ± 0.24	1.2 ± 0.2	0.7 ± 0.2
LATE	24	7.09 ± 0.27	0.1 ± 0.3	0.7 ± 0.3
$M_{\text{BH}}-M_{1\text{kpc}}$				
ALL	60	7.62 ± 0.18	1.8 ± 0.3	0.80 ± 0.3
EARLY	41	7.88 ± 0.20	2.0 ± 0.4	0.70 ± 0.2
LATE	19	7.06 ± 0.21	1.0 ± 0.4	0.70 ± 0.3
$M_{\text{BH}}-\sigma_*$				
ALL	109	8.33 ± 0.09	5.3 ± 0.3	0.5 ± 0.1
LATE	35	7.80 ± 0.20	3.4 ± 0.7	0.5 ± 0.2
EARLY	74	8.45 ± 0.10	4.9 ± 0.3	0.4 ± 0.1

Note. — We show fits to the $M_{\text{BH}}-M_{\text{tot}}$, the $M_{\text{BH}}-M_{1\text{kpc}}$ relation, and the $M_{\text{BH}}-\sigma_*$ relation using the Saglia et al. (2016) sample combined with the megamaser disks from this paper. Col. (1): Sample. LATE refers to all galaxies with Hubble Type later than S0, while EARLY includes elliptical and S0 galaxies. In all cases, we fit a linear model with $\log M_{\text{BH}}/M_\odot = \alpha + \beta \log(X/X_0) + \epsilon$, with X being M_{tot} ($X_0 = 10^{10} M_\odot$), $M_{1\text{kpc}}$ ($X_0 = 10^{10} M_\odot$), or σ_* ($X_0 = 200 \text{ km s}^{-1}$). Col. (2): Number of galaxies fitted. Col. (3): Zeropoint α (M_\odot). Col. (4): Slope β (M_\odot or km s^{-1}). Col. (5): Scatter ϵ .

4.2. Black Hole Mass and Stellar Velocity Dispersion

Turning to the $M_{\text{BH}}-\sigma_*$ relation, our linear fit to the full sample of galaxies confirms the steep slope found in recent works ($\beta = 5.3 \pm 0.3$) and the high intrinsic scatter ($\epsilon = 0.5 \pm 0.1$). In Greene et al. (2010), we found that the BH masses in the megamaser disk galaxies are lower than expected at a fixed σ_* . Here we double the megamaser disk sample and strongly confirm our previous result (Fig. 3). We calculate the average offset ΔM_{BH} between M_{BH} and that predicted by the $M_{\text{BH}}-\sigma_*$ relation fit to early-type galaxies. The offset is calculated as the weighted mean of the difference between the measured M_{BH} and that calculated from the best-fit relation, with the weights including both y and x uncertainties combined in quadrature (Läscher et al. 2016). We find an offset of -0.39 ± 0.12 for late-type galaxies and an offset of -0.45 ± 0.12 for pseudobulges⁷.

We now have marginally sufficient statistics to compare the distributions of maser and non-maser spirals. There are 20 megamaser disk galaxies (2 S0, 18 spiral) and 17 late-type (non-S0) spiral galaxies with M_{BH} measurements from non-maser dynamics. The maser and non-maser samples have indistinguishable distributions in σ_* according to an Anderson-Darling test (e.g., Babu & Feigelson 2006) with $p = 0.6$ of being drawn from the same distribution. Likewise, the distributions of bulge type are quite similar, with $\sim 75\%$ of the stellar/gas dynamical and $\sim 85\%$ of the megamaser disk galaxies hosted by pseudobulges (Table 1).

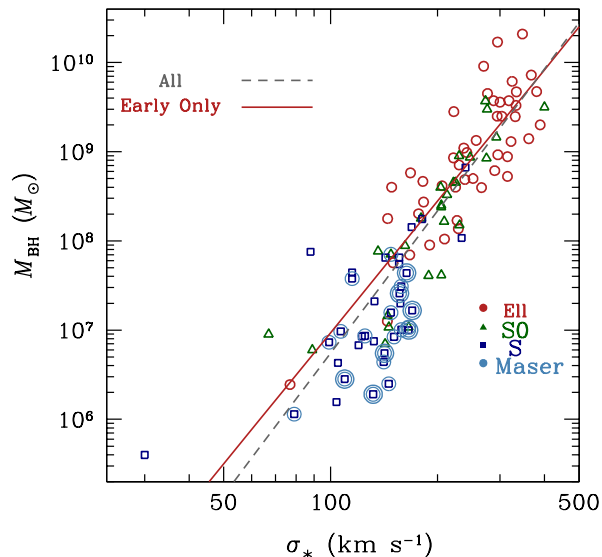


FIG. 3.— The relationship between σ_* and M_{BH} . We fit the entire sample (grey dashed line) and the early-type galaxies alone (red solid). Note the systematic offset to lower M_{BH} at a fixed σ_* for the megamaser disk galaxies. Symbols as in Figure 2.

Calculating the net offset from our best-fit $M_{\text{BH}}-\sigma_*$ relation for elliptical galaxies, we find $\Delta M_{\text{BH}} = -0.60 \pm 0.14$ dex for the 20 megamaser disks, while we find no mean offset $\Delta M_{\text{BH}} = -0.15 \pm 0.15$ dex for the non-maser spirals (Fig. 4). The maser and non-maser spirals are significantly different in $(M_{\text{BH}}/\sigma_*)^5$; the Anderson-Darling test returns a probability $P = 0.015$ that they are drawn from the same distribution (Fig. 4), even if we focus on just the 18 non-S0 maser disk galaxies or the maser and non-maser pseudobulge samples ($P = 0.01$). Finally, we examine the two samples non-parametrically in two dimensions using the Cramer Von-Mises test, and find that the two samples are different at 90% significance.

With such small numbers we see only a suggestive difference between the maser and non-maser samples. On the other hand, we see a similar trend in the $M_{\text{BH}}-M_{\text{bul}}$ relations (Läsaker et al. 2016). Thus, we briefly consider the possible ramifications should this difference prove real. There are three possibilities. First, the masers could trace the true M_{BH} distribution, while the non-maser M_{BH} distribution is biased due to the inability to resolve the sphere of influence of $< 10^7 M_{\odot}$ BHs. Existing upper limits do not constrain this possibility, as they are at higher BH mass (Gültekin et al. 2011). In this scenario, spiral (or low-mass) galaxies do have a broad range of M_{BH} , as may be expected in merger-driven scenarios (e.g., Jahnke & Macciò 2011) or if M_{BH} never gets large enough to exert feedback on the galaxy (e.g., Zubovas & King 2012).

Second, the non-maser distribution could be the real one, with masers preferentially occurring in lower- M_{BH} systems due to a correlation between M_{BH} and disk size (Neufeld et al. 1994; van den Bosch et al. 2016). The third possibility, which we view as highly unlikely, is that we may be preferentially catching the maser galaxies as they grow toward the $M_{\text{BH}}-\sigma_*$ relation. Given that BH growth episodes are likely quite short compared to the growth times of bulges (many Gyr), we do not favor this third scenario (Greene et al. 2010). We urgently need more obser-

vations of both spiral and elliptical galaxies at low mass, using multiple methods, to determine the full distribution of M_{BH} at low galaxy mass.

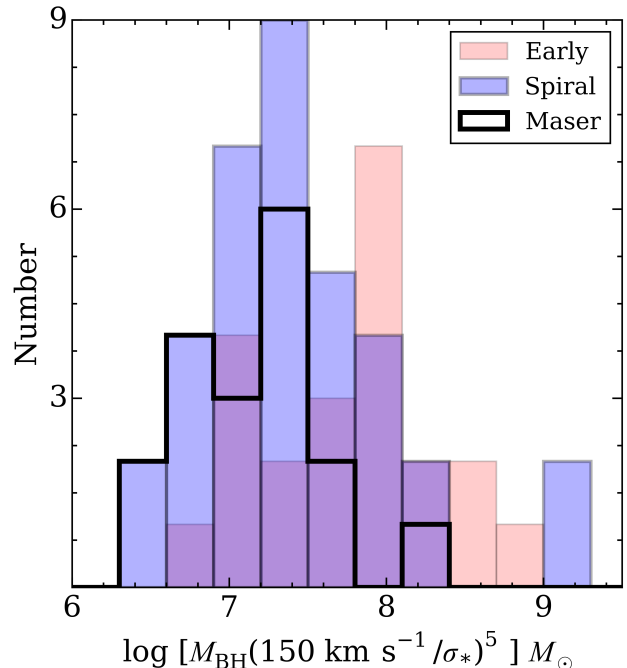


FIG. 4.— The distribution of M_{BH} at fixed σ_* . Megamaser galaxies (thick black) are offset to lower M_{BH} than the full sample of spirals (blue filled) or the early-type galaxies (red filled).

5. SUMMARY

We present new stellar velocity dispersion measurements for seven megamaser disk galaxies, and revisit galaxy-BH scaling relations that incorporate these new measurements. In addition to σ_* , we investigate total stellar mass M_* , and a non-parametric measure of central stellar mass density within 1 kpc, $M_{1\text{kpc}}$. We have also recently examined bulge mass (Läsaker et al. 2016), and halo mass (Sun et al. 2013).

The M_{BH} in megamaser disk galaxies span a large range for any fixed galaxy property, while the maser and non-maser dynamical measurements have different distributions of M_{BH} at a fixed galaxy property. To determine the real distribution of M_{BH} in this low-mass regime we must push the sphere-of-influence limit downwards for non-maser M_{BH} . We hope that with ALMA (e.g., Barth et al. 2016) and thirty-meter-class optical/NIR telescopes (e.g., Do et al. 2014), we will fill in low-mass galaxies with non-maser dynamical measurements to address the full distribution of M_{BH} in low-mass galaxies.

We thank the referee for a constructive report that significantly improved this manuscript. J.E.G. thanks A. Barth, K. Gültekin, S. Tremaine, and R. van den Bosch for useful discussions. J.E.G. acknowledges funding from NSF grant AST-1310405. ACS acknowledges support from NSF grant AST-1350389. This research has made use of the NASA/IPAC Extragalactic Database (NED) which is operated by the Jet Propulsion Laboratory, California Institute of Technology, under contract with the National Aeronautics and Space Administration.

REFERENCES

- Babu, G. J., & Feigelson, E. D. 2006, in *Astronomical Society of the Pacific Conference Series*, Vol. 351, *Astronomical Data Analysis Software and Systems XV*, ed. C. Gabriel, C. Arviset, D. Ponz, & S. Enrique, 127
- Barro, G., Faber, S. M., Koo, D. C., Dekel, A., Fang, J. J., Trump, J. R., Perez-Gonzalez, P. G., Pacifici, C., Primack, J. R., Somerville, R. S., Yan, H., Guo, Y., Liu, F., Ceverino, D., Kocevski, D. D., & McGrath, E. 2015, *ArXiv e-prints*
- Barth, A. J., Boizelle, B. D., Darling, J., Baker, A. J., Buote, D. A., Ho, L. C., & Walsh, J. L. 2016, *ApJ*, 822, L28
- Bell, E. F., McIntosh, D. H., Katz, N., & Weinberg, M. D. 2003, *ApJS*, 149, 289
- Bennert, V. N., Treu, T., Auger, M. W., Cosens, M., Park, D., Rosen, R., Harris, C. E., Malkan, M. A., & Woo, J.-H. 2015, *ApJ*, 809, 20
- Bezanson, R., van Dokkum, P. G., Täl, T., Marchesini, D., Kriek, M., Franx, M., & Coppi, P. 2009, *ApJ*, 697, 1290
- Cappellari, M., & Emsellem, E. 2004, *PASP*, 116, 138
- Cushing, M. C., Vacca, W. D., & Rayner, J. T. 2004, *PASP*, 116, 362
- Debuhr, J., Quataert, E., Ma, C.-P., & Hopkins, P. 2010, *MNRAS*, 406, L55
- den Brok, M., Seth, A. C., Barth, A. J., Carson, D. J., Neumayer, N., Cappellari, M., Debattista, V. P., Ho, L. C., Hood, C. E., & McDermid, R. M. 2015, *ApJ*, 809, 101
- Do, T., Wright, S. A., Barth, A. J., Barton, E. J., Simard, L., Larkin, J. E., Moore, A. M., Wang, L., & Ellerbroek, B. 2014, *AJ*, 147, 93
- Dunkley, J., et al. 2009, *ApJ*, 701, 1804
- Emsellem, E., et al. 2007, *MNRAS*, 379, 401
- Falcón-Barroso, J., Bacon, R., Bureau, M., Cappellari, M., Davies, R. L., de Zeeuw, P. T., Emsellem, E., Fathi, K., Krajnović, D., Kuntschner, H., McDermid, R. M., Peletier, R. F., & Sarzi, M. 2006, *MNRAS*, 369, 529
- Gao, F., Braatz, J. A., Reid, M. J., Lo, K. Y., Condon, J. J., Henkel, C., Kuo, C. Y., Impellizzeri, C. M. V., Pesce, D. W., & Zhao, W. 2016, *ApJ*, 817, 128
- Gebhardt, K., Richstone, D., Tremaine, S., Lauer, T. R., Bender, R., Bower, G., Dressler, A., Faber, S. M., Filippenko, A. V., Green, R., Grillmair, C., Ho, L. C., Kormendy, J., Magorrian, J., & Pinkney, J. 2003, *ApJ*, 583, 92
- Greene, J. E., Peng, C. Y., Kim, M., Kuo, C.-Y., Braatz, J. A., Impellizzeri, C. M. V., Condon, J. J., Lo, K. Y., Henkel, C., & Reid, M. J. 2010, *ApJ*, 721, 26
- Greene, J. E., Seth, A., Lyubenova, M., Walsh, J., van de Ven, G., & Läsker, R. 2014, *ApJ*, 788, 145
- Gültekin, K., Tremaine, S., Loeb, A., & Richstone, D. O. 2011, *ApJ*, 738, 17
- Horne, K. 1986, *PASP*, 98, 609
- Jahnke, K., & Macciò, A. V. 2011, *ApJ*, 734, 92
- Kelly, B. C. 2007, *ApJ*, 665, 1489
- Kormendy, J., & Ho, L. C. 2013, *ARA&A*, 51, 511
- Kuo, C. Y., Braatz, J. A., Condon, J. J., Impellizzeri, C. M. V., Lo, K. Y., Zaw, I., Schenker, M., Henkel, C., Reid, M. J., & Greene, J. E. 2011, *ApJ*, 727, 20
- Kuo, C. Y., Braatz, J. A., Lo, K. Y., Reid, M. J., Suyu, S. H., Pesce, D. W., Condon, J. J., Henkel, C., & Impellizzeri, C. M. V. 2015, *ApJ*, 800, 26
- Läsker, R., Greene, J. E., Seth, A., van de Ven, G., Braatz, J. A., Henkel, C., & Lo, K. Y. 2016, *ApJ*, accepted (arXiv/1602.06960)
- McConnell, N. J., & Ma, C.-P. 2013, *ApJ*, 764, 184
- Miralda-Escudé, J., & Kollmeier, J. A. 2005, *ApJ*, 619, 30
- Miyoshi, M., Moran, J., Herrnstein, J., Greenhill, L., Nakai, N., Diamond, P., & Inoue, M. 1995, *Nature*, 373, 127
- Neufeld, D. A., Maloney, P. R., & Conger, S. 1994, *ApJ*, 436, L127
- Pesce, D. W., Braatz, J. A., Condon, J. J., Gao, F., Henkel, C., Litzinger, E., Lo, K. Y., & Reid, M. J. 2015, *ApJ*, 810, 65
- Reines, A. E., & Volonteri, M. 2015, *ApJ*, 813, 82
- Roediger, J. C., & Courteau, S. 2015, *MNRAS*, 452, 3209
- Rusli, S. P., Erwin, P., Saglia, R. P., Thomas, J., Fabricius, M., Bender, R., & Nowak, N. 2013, *AJ*, 146, 160
- Saglia, R. P., Opitsch, M., Erwin, P., Thomas, J., Beifiori, A., Fabricius, M., Mazzalay, X., Nowak, N., Rusli, S. P., & Bender, R. 2016, *ApJ*, 818, 47
- Springel, V., Di Matteo, T., & Hernquist, L. 2005, *ApJ*, 620, L79
- Sun, A.-L., Greene, J. E., Impellizzeri, C. M. V., Kuo, C.-Y., Braatz, J. A., & Tuttle, S. 2013, *ApJ*, 778, 47
- Thomas, J., Ma, C.-P., McConnell, N. J., Greene, J. E., Blakeslee, J. P., & Janish, R. 2016, *Nature*, 532, 340
- Tremaine, S., Gebhardt, K., Bender, R., Bower, G., Dressler, A., Faber, S. M., Filippenko, A. V., Green, R., Grillmair, C., Ho, L. C., Kormendy, J., Lauer, T. R., Magorrian, J., Pinkney, J., & Richstone, D. 2002, *ApJ*, 574, 740
- Vacca, W. D., Cushing, M. C., & Rayner, J. T. 2003, *PASP*, 115, 389
- Valdes, F., Gupta, R., Rose, J. A., Singh, H. P., & Bell, D. J. 2004, *ApJS*, 152, 251
- van den Bosch, R. C. E., Gebhardt, K., Gültekin, K., Yıldırım, A., & Walsh, J. L. 2015, *ApJS*, 218, 10
- van den Bosch, R. C. E., Greene, J. E., Braatz, J. A., Constantin, A., & Kuo, C.-Y. 2016, *ApJ*, 819, 11
- Volonteri, M. 2010, *A&A Rev.*, 18, 279
- Wallace, L., & Hinkle, K. 1996, *ApJS*, 107, 312
- Walsh, J. L., van den Bosch, R. C. E., Gebhardt, K., Yıldırım, A., Gültekin, K., Husemann, B., & Richstone, D. O. 2015, *ApJ*, 808, 183
- Walsh, J. L., van den Bosch, R. C. E., Gebhardt, K., Yıldırım, A., Richstone, D. O., Gültekin, K., & Husemann, B. 2016, *ApJ*, 817, 2
- Wilson, J. C., Henderson, C. P., Herter, T. L., Matthews, K., Skrutskie, M. F., Adams, J. D., Moon, D.-S., Smith, R., Gautier, N., Ressler, M., Soifer, B. T., Lin, S., Howard, J., LaMarr, J., Stolberg, T. M., & Zink, J. 2004, in *Society of Photo-Optical Instrumentation Engineers (SPIE) Conference Series*, Vol. 5492, *Ground-based Instrumentation for Astronomy*, ed. A. F. M. Moorwood & M. Iye, 1295–1305
- York, D. G., et al. 2000, *AJ*, 120, 1579
- Zubovas, K., & King, A. R. 2012, *MNRAS*, 426, 2751